Correlation between nuclear charge radii of Ti and reaction cross sections for *p*-Ti

M. Hemalatha,[1,*] N. Maladkar,[1] and S. Kailas[1,2]
[1]*UM-DAE Centre for Excellence in Basic Sciences, Mumbai 400098, India*
[2]*Bhabha Atomic Research Centre, Mumbai 400085, India*
(Received 11 May 2015; published 17 August 2015)

The nuclear root-mean-square charge radii and nuclear density distributions have been calculated in the framework of relativistic self-consistent mean-field models based on density-dependent meson-exchange relativistic energy density functional for even isotopes of Ti ($A = 44-56$). The calculations agree well with available laser spectroscopic measurements for ^{44,46,48,50}Ti, and results for neutron-rich isotopes are reported. The semimicroscopic proton optical potentials for $^{44-56}$Ti have been derived by folding the target matter density with the extended Jeukenne-Lejeune-Mahaux energy- and density-dependent internucleon interaction and are used to calculate the differential elastic scattering and reaction cross sections at 65 MeV. The calculated differential cross sections reproduce the corresponding experimental values for stable even isotopes, and predictions are presented for ^{44,52,54,56}Ti. The calculations reveal a prominent kink at the $N = 28$ shell closure observed in the variation of reaction cross sections, consistent with mean-square charge radii systematics in the Ti isotopic chain.

DOI: 10.1103/PhysRevC.92.024611 PACS number(s): 21.10.−k, 21.60.Jz, 24.10.Ht, 25.40.Cm

I. INTRODUCTION

The study of structure and properties of nuclei far from the region of β stability and close to the drip lines has recently become feasible due to advances in the production of radioactive ion beams. It is important to determine shell effects and their influence on properties of nuclei, including charge radii. The trend of rms charge radii $\langle r_c^2 \rangle^{1/2}$ around shell closures $Z = 20$ (Ca) and $N = 28$ has been investigated through laser spectroscopic techniques [1–5] and also theoretically [6,7]. However, there is limited experimental information on charge radii in the vicinity of $N = 20$ and $N = 28$ shell closures [8]. The nuclear charge radius and reaction cross section can be correlated and useful information about nuclear structure can be extracted. For example, a remarkably large experimental reaction cross section of ^{11}Li, as compared to neighboring Li isotopes, was attributed to a correspondingly large increase in matter distribution [9]. Similarly, an large increase in experimental charge radii observed in the Zr isotopic chain was associated with an upturn in predicted reaction cross sections [10]. The Ti isotopic chain lies in an interesting region near $Z = 20$ and $N = 28$ shell gaps, and rms charge radii data are available only for stable ^{46,48,50}Ti isotopes and the neutron-deficient ^{44}Ti nucleus [5]. The correlation between rms charge radii and the reaction cross sections in Ti isotopes can be investigated by studying *p*-Ti elastic scattering. Elastic scattering differential cross section data for proton scattering at 65 MeV are available for ^{46,48,50}Ti [11]. In the present work, ground-state properties have been calculated for both neutron-deficient and neutron-rich even Ti isotopes. The correlation between rms charge radii and the reaction cross sections has been utilized to predict reaction cross sections for protons scattering from even isotopes $^{44-56}$Ti. The predictions of the differential elastic scattering and reaction cross sections for unstable isotopes can be validated by performing proton elastic scattering in inverse kinematics in the present radioactive ion-beam facilities.

The ground-state properties are calculated in the framework of self-consistent mean-field models based on relativistic energy density functionals [12] using the interaction DD-ME2 [13] for even Ti isotopes. The binding energies, neutron separation energies, and charge radii have been calculated and compared with the corresponding data, where available. The target matter densities with the above prescription have been used in the semimicroscopic optical model to obtain the proton optical potentials for even Ti isotopes. For this purpose, target matter densities are folded with the extended Jeukenne-Lejeune-Mahaux (JLM) energy- and density-dependent nucleon-nucleon interaction [14,15]. The resulting real and imaginary parts of the optical potential are used to compute the reaction and differential cross sections for 65 MeV proton scattering from even Ti isotopes.

The details of the formulation employed in the calculation of ground-state properties are presented in Sec. II, along with the results for even isotopes of Ti. Section III describes the semimicroscopic optical model calculation of the folded potential. The calculated differential and reaction cross section for 65 MeV proton scattering from even Ti isotopes and comparison with the available data are also presented in the same section.

II. RELATIVISTIC SELF-CONSISTENT MEAN-FIELD FRAMEWORK

The self-consistent mean-field structure models based on relativistic (covariant) energy density functionals are employed. Various aspects of nuclear structure, in isotopes ranging from stable ones to those approaching the nucleon drip line, have been satisfactorily explained by models employing the Relativistic Mean Field (RMF) approach [16,17]. The predictions are comparable to those using the nonrelativistic Hartree-Fock-Bogoliubov approach based on Skyrme functionals or Gogny effective interactions [17–20]. In

*hema@cbs.ac.in

conventional quantum hydrodynamics, a nucleus is considered as a system of Dirac nucleons coupled to exchange mesons through an effective Lagrangian. The isoscalar-scalar σ meson, the isoscalar-vector ω meson, and the isovector-vector ρ meson build the minimal set of meson fields necessary for a description of bulk and single-particle nuclear properties. Calculations are performed with the density-dependent meson-exchange relativistic energy functional, DD-ME2 [13], which is found to provide a good description. The particle-particle channel of the effective internucleon interaction is described by a separable finite-range pairing force [21].

The Relativistic Hartree Bogoliubov (RHB) equation is solved in the configuration space of harmonic oscillator wave functions with appropriate symmetry, whereas the densities are computed in coordinate space. The method has been applied to spherical as well as axially and nonaxially deformed nuclei. The diagonalization of the RHB matrix equation yields the wave functions in configuration space. The resulting density matrix is then transformed to coordinate space, and the resulting vector and scalar densities are used to calculate the potentials. It should be noted that the procedure to adjust the energy density functional parameters for the DD-ME2 set involves treating the pairing correlations in the BCS constant-gap approximation with empirical pair gaps (5-point formula) [22]. In the case of axial symmetry the solution of the Helmholtz equations for the meson fields is obtained by expanding in a harmonic oscillator basis. The details of the solution of the RMF equations are given in Ref. [23].

In the present work, the RHB calculations using DD-ME2 are denoted by DIRHB. The DIRHB results for physical observables like the binding energies, charge radii, and proton and neutron densities for even Ti isotopes are discussed below.

A. Calculation of charge radii

The mean-square charge radius $\langle r_c^2 \rangle$ is obtained from the proton density $\rho_p(r)$ (normalized to unity) [24] given by the relation,

$$\langle r_c^2 \rangle = \int r^2 \rho_p(r) d^3r + \langle r_p^2 \rangle - \frac{N}{Z} \langle r_n^2 \rangle,$$

where $\langle r_p^2 \rangle$ and $\langle r_n^2 \rangle$ denote the mean-square radius of the point-proton and point-neutron density distributions, respectively.

Before going into detail about the calculated charge radii, we compare the calculated binding energies and two neutron separation energies with data, where available, for even Ti isotopes. The calculated binding energies for even Ti isotopes are found to be within 1% of corresponding experimental values [25]. Further, experimental values of two neutron separation energies [25] are reproduced by calculations, and the shell closure for ^{50}Ti ($N = 28$) is clearly evident.

The calculated change in the rms charge radii relative to $N = 28$ (^{50}Ti), $\delta\langle r_c^2 \rangle^{N,28}$, is shown in Fig. 1 for even isotopes of Ti. Experimental values [11] for $\delta\langle r_c^2 \rangle^{N,28}$ are available for ^{44,46,48,50}Ti. The calculated $\delta\langle r_c^2 \rangle^{N,28}$ agree quite well with the corresponding measured values [5]. For comparison, $\delta\langle r_c^2 \rangle^{N,28}$ calculated using droplet model [26] are also shown in Fig. 1. It is seen that the droplet model calculations for $\delta\langle r_c^2 \rangle^{N,28}$ for all

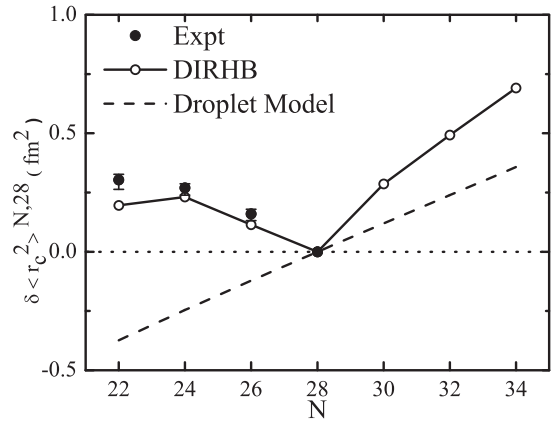

FIG. 1. Calculated DIRHB rms charge radii relative to $N = 28$ (^{50}Ti) for even Ti isotopes. The corresponding experimental values [5] (where available) are shown for comparison. The dashed line indicates $\delta\langle r_c^2 \rangle^{N,28}$ values obtained using droplet model [26].

isotopes are lower compared to those obtained from DIRHB. A steady increase in DIRHB calculated $\delta\langle r_c^2 \rangle^{N,28}$ values with the addition of neutrons is seen for neutron-rich isotopes. While in the neutron-deficient region, both calculation and experiment show a different behavior, i.e., removal of two neutrons from $N = 28$ increases $\delta\langle r_c^2 \rangle^{N,28}$, instead of the decrease expected from the droplet model estimate. The calculations indicate that ^{46}Ti has similar radius to that of ^{52}Ti. It is also seen that as neutrons are removed from ^{50}Ti, the $\delta\langle r_c^2 \rangle^{N,28}$ increases smoothly up to ^{46}Ti followed by a change in slope at $N = 24$. The trend in variation of $\langle r_c^2 \rangle^{1/2}$ can be explained in terms of the change in charge radii as a function of quadrupole deformation [27]. It is well-known that the mid-neutron shell nuclei have maximum deformation. The DIRHB calculation shows maximum quadrupole deformation for mid-neutron shell nucleus ^{46}Ti, and this behavior is reflected in the calculated $\delta\langle r_c^2 \rangle^{N,28}$ values.

B. Calculated density distributions

Following the agreement with experimental data of calculated ground-state properties, we now calculate the point proton and neutron density distributions that are required for the calculation of semimicroscopic optical model potential. The $L = 0$ projected and renormalized DIRHB point proton and neutron density distributions calculated for the even Ti isotopes $^{44-56}$Ti are shown in Fig. 2. Proton and neutron density distributions (ρ_p and ρ_n) are quite similar for all the nuclei in the interior region. In the surface region, ρ_p exhibits a different trend as compared to ρ_n. ρ_p has the least spread for ^{50}Ti, while it is more extended and similar in nature for ^{44,46}Ti; also ρ_p for ^{48,52,54,56}Ti closely resemble one another. ρ_n for ^{44,46,48,50}Ti are similar and extend over smaller distances as compared to those for ^{52,54,56}Ti. The DIRHB point proton and neutron density distributions calculated for the even Ti isotopes are used in the folding model analysis, which is discussed in the next section.

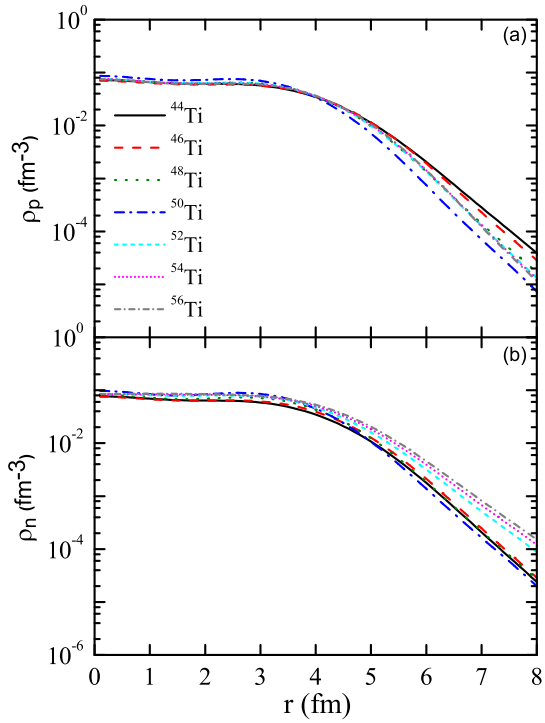

FIG. 2. (Color online) Calculated DIRHB ($L = 0$ projected and renormalized) (a) proton densities and (b) neutron densities for even Ti isotopes.

III. SEMIMICROSCOPIC OPTICAL MODEL

The elastic scattering calculation using folding model serves to relate the cross sections with nuclear structure information of the proton and neutron density distributions. This is achieved by fixing the parameters of the effective interaction in the folding model analysis and the differences in nuclear density distribution among the isotopes are probed. In the energy range of interest (typically 50–100 MeV) and for systems p-A and n-A, the JLM model predictions for scattering and reaction observables assuming spherical symmetry work well when the radial matter densities are obtained from well-established structure models whether relativistic or nonrelativistic [28,29]. Similar considerations hold for other microscopic, spherical nucleon-nucleus optical model potentials based on different approximations or effective forces [30,31]. In the present work, the optical model potential (OMP) [14,15] is built by folding the extended JLM interaction with the target radial matter densities. The point proton and neutron densities used here are calculated in DIRHB framework using DD-ME2 interaction as described in the previous section. The OMP in nuclear matter is based on the Brückner-Hartree-Fock work of JLM and the interaction is spin independent as well as energy and density dependent. The imaginary part of the effective interaction is multiplied by an effective mass. To make the JLM interaction which has been established for nuclear matter relevant to finite nuclei, a local density approximation (LDA) is applied. The LDA is further improved and extended to deformed nuclei [15]. In the absence of spin-orbit interaction in JLM model, we have used the phenomenological prescription [32] to calculate the deformed complex spin-orbit potential in the full Thomas form [15]. Using the real and imaginary parts of the proton optical model potential, the differential and reaction cross sections are calculated. This semimicroscopic approach is used in the analysis of proton elastic scattering on even Ti isotopes ($A = 44-56$). In the present work, we have not considered the coupled channel effects for deformed Ti isotopes. These effects are significant at lower energies and are expected to be less important at the energy (65 MeV) considered here. It is seen that Ti isotopes, except those with $N = 20$ and $N = 28$, are open shell nuclei and collectivity sets in Refs. [33,34].

A. Calculated folded potentials

The real and imaginary parts of the central and spin-orbit potentials are obtained by folding the JLM internucleon interaction with the calculated DIRHB densities using the computer code MOM (microscopic optical model) [15] for 65 MeV proton elastic scattering from even isotopes of Ti. The code ECIS [35] is used to calculate the differential and reaction cross sections and for performing χ^2 minimization by fitting the differential cross section to corresponding data. Good agreement to differential cross section data [11] for stable even Ti isotopes has been possible with overall renormalization of the real and imaginary parts of the central potential and real part of the spin-orbit one. The imaginary part of the spin-orbit potential was not used in the calculation as it did not have a significant influence on the cross section results. The renormalization factors for real (λ_V) and imaginary central (λ_W) and real spin-orbit ($\lambda_{V\mathrm{so}}$) parts of the potential, for the stable even isotopes of Ti, were obtained by performing a search to achieve a minimum χ^2 in fitting the differential cross section data [11]. To reduce the number of parameters for prediction of cross sections, the values of $\lambda_{V\mathrm{so}}$ obtained from search for stable isotopes, was fixed to the average value of $\lambda_{V\mathrm{so}} = 88$. It was seen that with $\lambda_{V\mathrm{so}}$ fixed to 88, and λ_V and λ_W both obtained from the search, resulted in a good fit to the differential cross section data for stable isotopes, ^{46,48,50}Ti; these are referred to as best fit values (Fig. 4). Using these best fit values, the calculated renormalized real central V(r), imaginary central W(r) and real spin-orbit V_{so}(r) parts of the folded potential are plotted in Fig. 3 for the stable isotopes. Figure 3 also shows the corresponding phenomenological parts of the Woods-Saxon (WS) potential [11]. It is clear from figure that for ^{46,48,50}Ti, in general, the semimicroscopic calculation for real and imaginary central, and real spin-orbit parts of the potential are similar to the corresponding WS parts of the potential, with the exception of V(r) in the interior region for ^{50}Ti.

A least-squares fit to the best fit values of λ_V and λ_W has been carried out to obtain the renormalization constants for even neutron-deficient and neutron-rich Ti isotopes. These are shown in Fig. 4 by solid lines. This figure reveals a small dependence on A of both λ_V and λ_W and their variation is given in terms of the expressions: $\lambda_V = 0.0228A - 0.193$ and $\lambda_W = 0.0847A - 3.210$, respectively. The λ_V values are close to unity for all the isotopes under consideration. For the sake of completeness, we note the average of the best fit λ_V and λ_W values obtained from ^{46,48,50}Ti to be 0.90 and 0.86,

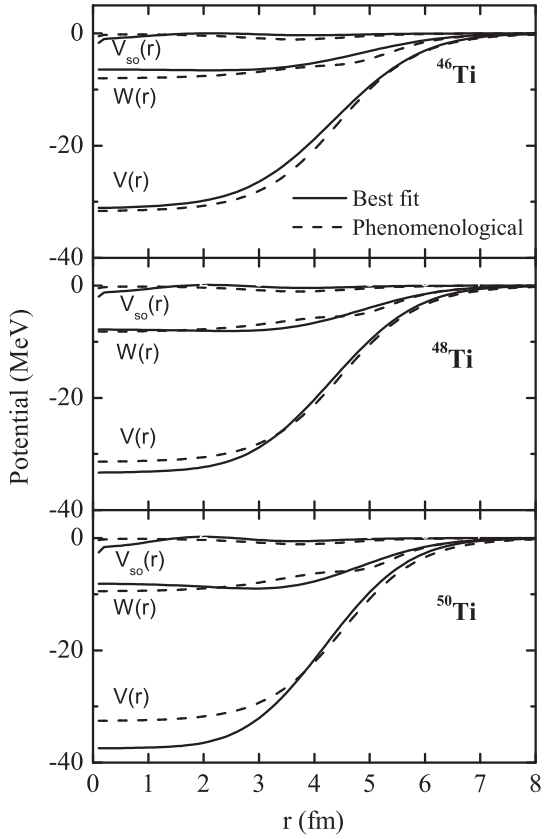

FIG. 3. Renormalized real central, imaginary central and real spin-orbit parts of the folded potential using best fit values of λ_V and λ_W for (p,p) scattering from stable even Ti isotopes. The corresponding phenomenological [11] Woods-Saxon (WS) potentials are also shown.

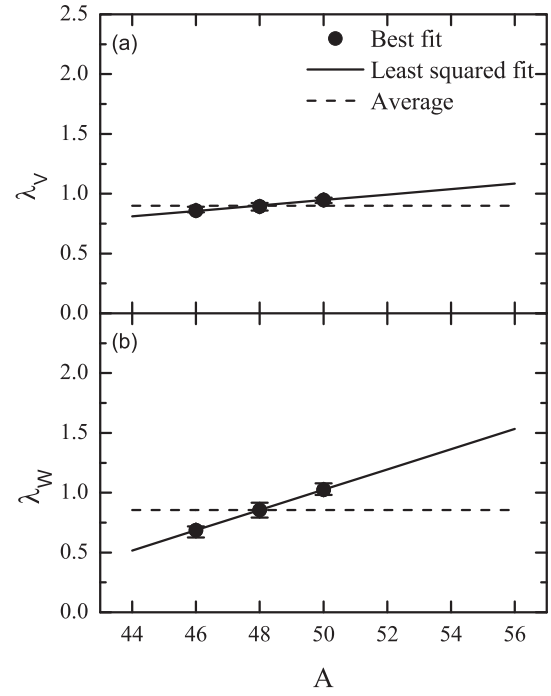

FIG. 4. Renormalization constants for (a) real and (b) imaginary central parts of the potential obtained from the present MOM calculation for (p,p) scattering from even Ti isotopes. The λ_V and λ_W values from least-squares fit and average values are shown by solid and dashed lines, respectively for $^{44-56}$Ti. The corresponding best fit values for stable isotopes ^{46,48,50}Ti are shown by solid circles.

respectively, and these are plotted in Fig. 4 as a function of A. The best fit values of λ_V and λ_W are also shown in the Fig. 4. The errors in λ_V and λ_W are obtained by changing λ_V and λ_W, respectively, to get a variation in χ^2 by a factor of 2 from the respective best fit values.

In the next section, we discuss the calculation of cross sections using best fit, least-squares fit, and average values of λ_V and λ_W, with $\lambda_{V\mathrm{so}}$ fixed.

B. Calculated cross sections

Predictions of differential and reaction cross sections for neutron-deficient and neutron-rich even isotopes ($^{44-56}$Ti) are made with the calculated optical model potential obtained in the previous section as inputs to the ECIS code [35]. The calculation of cross sections using least-squares fit and average values of λ_V and λ_W with $\lambda_{V\mathrm{so}}$ are denoted by sets I and II, respectively. The calculated differential cross sections for the elastic scattering of 65 MeV proton incident on Ti isotopes are displayed in Fig. 5. In the figure, the set I calculations are shown. The experimental differential cross section [11] for the stable isotopes are also indicated in the same figure. The semimicroscopic calculations are in good agreement with the corresponding data. The calculated angular distributions are seen to shift slightly to lower angles and the minima become increasingly deeper with addition of neutrons.

The calculated total reaction cross sections σ_R using both least-squares fit (set I) and average (set II) values of λ_V and λ_W for even Ti isotopes are depicted in Fig. 6. The calculated σ_R using the best fit values of λ_V and λ_W obtained for stable isotopes are also plotted in the same figure. For comparison, both geometric σ_R^g and cross section σ_R^k from an improved parametrization in the Kox model [36,37] which is based on the strong absorption model are shown in Fig. 6. The geometric cross section are calculated as per the relation $\sigma_R^g = \pi r_0^2 (A_p^{1/3} + A_{\mathrm{Ti}}^{1/3})^2$, where A_p and A_{Ti} are the mass of the projectile p and Ti target, respectively. The σ_R^g and σ_R^k are both normalized to the σ_R calculated from best fit values of λ_V and λ_W for ^{50}Ti, and are also included in the figure. Both σ_R^g and σ_R^k show a smooth increase with N and the kink seen in the DIRHB calculated σ_R is not present at $N = 28$. σ_R^k has a larger slope in comparison with σ_R^g and shows better agreement with set I calculation for σ_R. In the neutron-rich region, σ_R from the set I calculations are significantly larger than the geometrical predictions while below $N = 26$ they are suppressed. The set II calculations for σ_R are found to be closer to the geometric cross sections for all isotopes. The total reaction cross section for 65 MeV proton scattering off ^{50}Ti obtained from the set I calculation is 836 mb. While the experimental σ_R at 65 MeV is not available, it may be noted that a value of $\sigma_R = 853 \pm 80$ mb [38] has been measured for scattering at 60.8 MeV protons off ^{50}Ti. The errors on σ_R are calculated by a similar procedure as

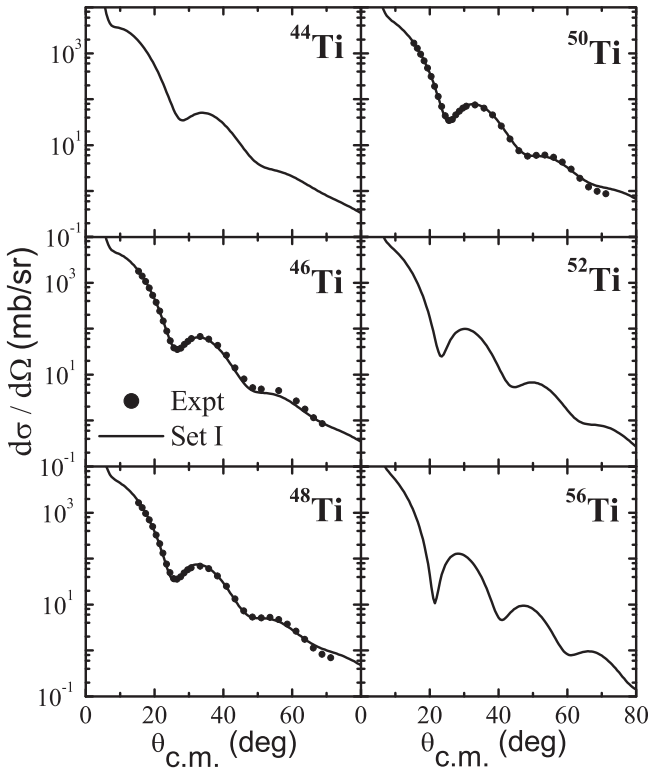

FIG. 5. Calculated (set I) and experimental [11] (where available) differential elastic scattering cross section for 65 MeV proton scattering from selected even Ti isotopes.

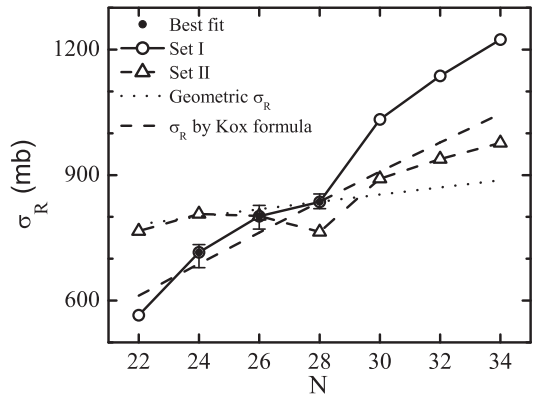

FIG. 6. Calculated total reaction cross section σ_R for 65 MeV proton scattering from even Ti isotopes. The σ_R are calculated using the best fit, least-squares fit (set I) and average (set II) values of λ_V and λ_W. Geometric cross sections and σ_R from Kox model are indicated by dotted and dashed lines, respectively.

that adopted for λ_V and λ_W. The calculations with both sets I and II show a smooth increase in σ_R as a function of A, with a sudden change of slope at shell closure, $N = 28$. Both calculations show a noticeable increase in σ_R going from ^{50}Ti to ^{52}Ti, consistent with mean-square charge radii systematics (Fig. 1).

IV. CONCLUSION

We have calculated the ground-state properties in the framework of self-consistent mean-field models based on relativistic energy density functionals using the interaction DD-ME2, for even isotopes $^{44-56}$Ti. The calculated rms charge radii are found to agree well with the available data and predictions have been made for neutron-rich isotopes of Ti up to $A = 56$. The calculated DIRHB densities are folded with the extended JLM, energy- and density-dependent nucleon-nucleon interaction to yield the optical potential which is then used to obtain the differential elastic scattering and reaction cross sections for 65 MeV proton scattering by even Ti isotopes. The differential cross sections obtained from the semimicroscopic calculations agree quite well with the corresponding experimental values for stable even isotopes, and predictions are presented for ^{44,52,54,56}Ti. Predictions of reaction cross sections have been made for even isotopes $^{44-56}$Ti, where no data are available. Our semimicroscopic calculation reveals a kink at $N = 28$ in the variation of total reaction cross section which is also reflected in the pronounced increase in the calculated rms charge radii for Ti isotopes. It would be interesting to verify predictions of total reaction cross sections for protons scattering from both neutron-deficient and neutron-rich Ti isotopes in the present radioactive ion-beam facilities.

ACKNOWLEDGMENTS

M.H. wishes to express gratitude to Profs. T. Nikšić and D. Vretenar for guidance in the calculation of nuclear ground-state properties. We thank Prof. Y. K. Gambhir for the critical reading of the manuscript and useful comments. S.K. would like to acknowledge support by Raja Ramanna fellowship from Board of Research in Nuclear Sciences, Department of Atomic Energy, Government of India.

[1] K. Kreim *et al.*, Phys. Lett. B **731**, 97 (2014).
[2] M. Avgoulea *et al.*, J. Phys. G: Nucl. Part. Phys. **38**, 025104 (2011).
[3] F. C. Charlwood *et al.*, Phys. Lett. B **690**, 346 (2010).
[4] K. Blaum, W. Geithner, J. Lassen, P. Lievens, K. Marinova, and R. Neugart, Nucl. Phys. A **799**, 30 (2008).
[5] Yu. P. Gangrsky and K. P. Marinova, J. Phys. G: Nucl. Part. Phys. **30**, 1089 (2004).
[6] G. A. Lalazissis, A. R. Farhan, and M. M. Sharma, Nucl. Phys. A **628**, 221 (1998).
[7] E. Caurier, K. Langanke, G. Martónez-Pinedo, F. Nowacki, and P. Vogel, Phys. Lett. B **522**, 240 (2001).
[8] I. Angeli and K. P. Marinova, At. Data Nucl. Data Tables **99**, 69 (2013).
[9] I. Tanihata, H. Hamagaki, O. Hashimoto, Y. Shida, N. Yoshikawa, K. Sugimoto, O. Yamakawa, T. Kobayashi, and N. Takahashi, Phys. Rev. Lett. **55**, 2676 (1985).
[10] M. Hemalatha, A. Bhagwat, A. Shrivastava, S. Kailas, and Y. K. Gambhir, Phys. Rev. C **70**, 044320 (2004).

[11] H. Sakaguchi, M. Nakamura, K. Hatanaka, A. Goto, T. Noro, F. Ohtani, H. Sakamoto, H. Ogawa, and S. Kobayashi, Phys. Rev. C **26**, 944 (1982).
[12] T. Nikšić, N. Paar, D. Vretenar, and P. Ring, Comput. Phys. Commun. **185**, 1808 (2014).
[13] G. A. Lalazissis, T. Nikšić, D. Vretenar, and P. Ring, Phys. Rev. C **71**, 024312 (2005).
[14] J. P. Jeukenne, A. Lejeune, and C. Mahaux, Phys. Rev. C **16**, 80 (1977).
[15] E. Bauge, J. P. Delaroche, and M. Girod, Phys. Rev. C **63**, 024607 (2001).
[16] T. Nikšić, D. Vretenar, and P. Ring, Prog. Part. Nucl. Phys. **66**, 519 (2011).
[17] D. Vretenar, A. V. Afanasjev, G. A. Lalazissis, and P. Ring, Phys. Rep. **409**, 101 (2005).
[18] M. Bender, P.-H. Heenen, and P.-G. Reinhard, Rev. Mod. Phys. **75**, 121 (2003).
[19] J. Meng, H. Toki, S. G. Zhou, S. Q. Zhang, W. H. Long, and L. S. Geng, Prog. Part. Nucl. Phys. **57**, 470 (2006).
[20] N. Paar, D. Vretenar, E. Khan, and G. Coló, Rep. Prog. Phys. **70**, 691 (2007).
[21] Yuan Tian, Zhongyu Ma, and P. Ring, Phys. Lett. B **676**, 44 (2009).
[22] P. Möller and J. R. Nix, Nucl. Phys. A **536**, 20 (1992).
[23] Y. K. Gambhir, P. Ring, and A. Thimet, Ann. Phys. (NY) **198**, 132 (1990).
[24] R. C. Barrett and D. F. Jackson, *Nuclear Sizes and Structure* (Clarendon Press, Oxford, 1977).
[25] M. Wang and G. Audi, Chin. Phys. C **36**, 1603 (2012).
[26] W. D. Myers and K.-H. Schmidt, Nucl. Phys. A **410**, 61 (1983).
[27] I. Angeli and K. P. Marinova, J. Phys. G: Nucl. Part. Phys. **42**, 055108 (2015).
[28] M. Arnould and S. Goriely, Nucl. Phys. A **777**, 157 (2006).
[29] M. Arnould, S. Goriely, and K. Takahashi, Phys. Rep. **450**, 97 (2007).
[30] M. Hemalatha, Y. K. Gambhir, W. Haider, and S. Kailas, Phys. Rev. C **79**, 057602 (2009).
[31] D. Pachouri, Syed Rafi, and W. Haider, J. Phys. G: Nucl. Part. Phys. **39**, 055101 (2012).
[32] R. R. Scheerbaum, Nucl. Phys. A **257**, 77 (1976).
[33] H. Suzuki *et al.*, Phys. Rev. C **88**, 024326 (2013).
[34] A. Gade *et al.*, Phys. Rev. Lett. **112**, 112503 (2014).
[35] J. Raynal, Phys. Rev. C **23**, 2571 (1981).
[36] S. Kox *et al.*, Phys. Rev. C **35**, 1678 (1987).
[37] L. Sihver, M. Lantz, and A. Kohama, Phys. Rev. C **89**, 067602 (2014).
[38] J. J. H. Menet, E. E. Gross, J. J. Malanify, and A. Zucker, Phys. Rev. C **4**, 1114 (1971).